Biochemistry

pubs.acs.org/biochemistry Article

Exploring the Mechanism of Covalent Inhibition: Simulating the Binding Free Energy of α-Ketoamide Inhibitors of the Main Protease of SARS-CoV-2

Dibyendu Mondal and Arieh Warshel*

Cite This: https://dx.doi.org/10.1021/acs.biochem.0c00782 Read Online

ACCESS | Metrics & More | Article Recommendations | Supporting Information

ABSTRACT: The development of reliable ways of predicting the binding free energies of covalent inhibitors is a challenge for computer-aided drug design. Such development is important, for example, in the fight against the SARS-CoV-2 virus, in which covalent inhibitors can provide a promising tool for blocking M^{pro}, the main protease of the virus. This work develops a reliable and practical protocol for evaluating the binding free energy of covalent inhibitors. Our protocol presents a major advance over other approaches that do not consider the chemical contribution of the binding free energy. Our strategy combines the empirical valence bond method for evaluating the reaction energy profile and the PDLD/S-LRA/β method for evaluating the noncovalent part of the binding process. This protocol has been used in the calculations of the binding free energy of an α-ketoamide inhibitor of M^{pro}. Encouragingly, our approach reproduces the observed binding free energy. Our study of covalent inhibitors of cysteine proteases indicates that in the choice of an effective warhead it is crucial to focus on the exothermicity of the point on the free energy surface of a peptide cleavage that connects the acylation and deacylation steps. Overall, we believe that our approach should provide a powerful and effective method for *in silico* design of covalent drugs.

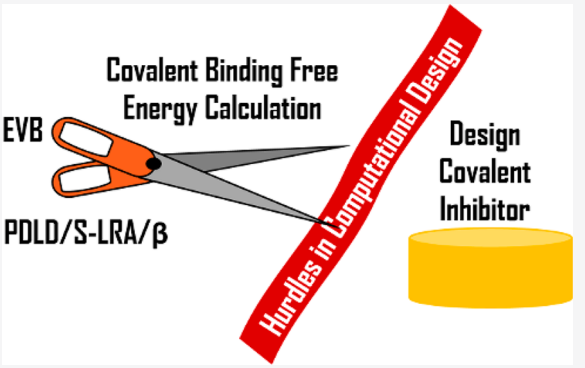

From December 2019, the whole world has been facing the problem of a highly contagious pulmonary disease, coronavirus disease 2019 (COVID-19).[1] Almost 41 million people in the world have been infected by this virus so far. The first case of this global pandemic was reported in the city of Wuhan, China.[2] The coronavirus strain severe acute respiratory syndrome coronavirus 2 (SARS-CoV-2)[3] is responsible for this global pandemic. So far, no vaccine or antiviral drug has been approved to prevent the spread of the SARS-CoV-2 system. Many proteins in SARS-CoV-2 have been targeted in the design of new drugs or the repurposing of known drugs,[4] and the main protease of SARS-CoV-2 (SARS-CoV-2 M^{pro}, also called $2CL^{pro}$)[5] is one of those. SARS-CoV-2 M^{pro} is a cysteine protease (CP) that takes part in the viral replication process. This protein cleaves the polyprotein pp1a and pp1ab (translated from the viral RNA) at 16 different positions to generate important structural (spike, envelope, membrane, and nucleocapsid proteins) as well as nonstructural proteins (NSPs).[6] Thus, hindering the normal action of M^{pro} can stop the spread of SARS-CoV-2. SARS-CoV-2 M^{pro} has a unique recognition sequence [Leu-Gln↓(Ser, Ala, Gly)], and the cleavage site (denoted by ↓) is between the Gln and the next small amino acid (Ser, Ala, or Gly).[7] No human proteases have this cleavage specificity, and as a result, inhibitors for SARS-CoV-2 M^{pro} are less likely to be toxic. This makes the M^{pro} an excellent target for drug design. Some crystal structures[7−10] of inhibitor-bound SARS-CoV-2 M^{pro} have been determined recently, and have immensely helped in the identificaton of important protein residues near the inhibitors. Most of those published crystal structures contain covalent inhibitors.

Generally, covalent inhibitors are more potent than their noncovalent analogues, because they form covalent bonds with the proteins. In fact, there are many examples of covalent inhibitors, particularly for protease enzymes.[11] For example, very recently a few potential broad-spectrum covalent inhibitors against alphacoronavirus, betacoronavirus, and enterovirus were reported.[12] These inhibitors bind specifically to the main proteases of those viruses. Unfortunately, most of these designs of covalent inhibitors are solely based on experimental studies, and computational research is yet to play a significant role. Reasonably accurate computational methods[13,14] are available for obtaining relative binding free

Received: September 22, 2020
Revised: October 20, 2020

https://dx.doi.org/10.1021/acs.biochem.0c00782
Biochemistry XXXX, XXX, XXX−XXX

energies of noncovalent inhibitors, but the main hurdle in developing computational approaches for designing covalent inhibitors is the simulation of the formation of the covalent bond. Unlike noncovalent inhibitors, the process of binding of a covalent inhibitor depends not only on the correct structural complementarity between the protein and the inhibitor but also the appropriate chemical reactivity of the inhibitor and the protein environment that stabilizes the covalent complex. Thus, designing good covalent inhibitors requires understanding the energy contributions of different steps in the covalent complex formation, which includes both the noncovalent binding free energy and the reaction free energies. In the past few years, several interesting computational studies have been reported,[15−18] where free energy perturbation (FEP)-based alchemical transformations were used in calculating the relative binding free energies of various covalent inhibitors. While in most of these works the noncovalent and covalent states were considered, the authors of ref 17 used only the covalent state in their calculations. As pointed out in ref 19, the choice of considering just the covalent state is reasonable only when the contribution of the covalent state to the total binding free energy is at least −5.5 kcal/mol greater than that of the noncovalent state. Unfortunately, knowing *a priori* the contributions from the covalent and noncovalent states is not possible. Thus, even for relative covalent binding free energy calculations, both contributions should be calculated. The situation gets even further complicated when one tries to calculate the absolute covalent binding free energies, because in this case the possibility of error cancelation (as we might expect in relative free energy calculations) is negligible. One might still be able to calculate the absolute binding free energies by considering one inhibitor as a reference and following the thermodynamic cycle used in ref 19 to avoid the expensive quantum mechanics (QM)-based calculations. On the contrary, a complete mechanistic understanding of the covalent inhibition process is not possible from such analysis. In fact, sometimes the inhibition is correlated with the transition state binding energy. Furthermore, comparison of different covalent warheads requires explicit evaluation of the chemical bonding process. Thus, it seems to us that there is a need for a protocol that is computationally less expensive but accurate enough [in terms of both the convergence and the reliability of the quantum mechanics/molecular mechanics (QM/MM) approach] in calculating both noncovalent binding free energies and reaction free energies.

We have previously combined the semimicroscopic version of the protein dipole Langevin dipole method in the linear response approximation with a scaled non-electrostatic term (PDLD/S-LRA and PDLD/S-LRA/β)[20] and the empirical valence bond (EVB)[21] method to investigate the drug resistance of the hepatitis C virus (HCV).[22] In that project, the PDLD/S-LRA method was used to calculate the noncovalent binding free energies of the substrate and inhibitors whereas EVB was employed to investigate the peptide hydrolysis mechanism. Thus, it is likely that we can combine these methods also to calculate absolute covalent binding free energies of inhibitor−protein complexes.

Considering the current pandemic situation, it is also very timely to try to use computer simulations to gain a detailed atomistic understanding of the inhibitor binding to SARS-CoV-2 M^{pro}. Such simulations can accelerate the design of new drugs to combat COVID-19 or other similar viruses that may be developed in the future.

In this paper, we have used the case of an α-ketoamide inhibitor (a reversible covalent inhibitor of M^{pro}) to explore the mechanism of inhibition of M^{pro}. Recently, the mechanism of proteolysis of the wild type substrate (polypeptide chain) by SARS-CoV-2 M^{pro} has been explored computationally.[23,24] These studies are very informative for designing new drugs, but understanding the mechanism of inhibition of SARS-CoV-2 M^{pro} by a covalent inhibitor would surely help more in the inhibitor design process.

The main protease of SARS-CoV-2 contains a cysteine (Cys145) and a histidine (His41) as a catalytic dyad [numbering based on the protomer chain A of the Protein Data Bank (PDB) entry 6Y2G[7]]. There are some proposals that the dyads of cysteine protease systems are already in the thiolate−imidazolium ion pair state in the apo form[25] of the proteins, and thus, upon substrate (or inhibitor) binding, the activated Cys can attack the most electrophilic center of the substrate (or inhibitor). An alternative proposal is that the Cys-His catalytic dyad remains in neutral form in the apo form of the protein and upon substrate (or inhibitor) binding the histidine residue activates the cysteine by abstracting the proton from its Sγ atom.[26,27] The activated cysteine then attacks the substrate (or inhibitor). In ref 23, a third mechanistic proposal was reported, where after substrate (or inhibitor) binding the proton transfer can occur concomitant with the next nucleophilic attack step.[23] All of the proposed mechanistic options mentioned above were considered in this work to investigate the inhibition process and are depicted in Figure 1. In schemes A and B, the nucleophilic attack (NA) occurs after the first proton transfer step (PT1) is completed, and those two steps occur in a concerted manner in scheme C. The last proton transfer step is the same for all of the schemes. The difference between schemes A and B is in the ordering of the PT1 and the inhibitor binding process (see Figure 1). To calculate the change in free energy for different steps in Figure 1, the PDLD/S-LRA/β or EVB method was utilized (depending upon the step). Furthermore, our calculated results have been compared to the experimental results and the most exothermic step in the entire binding process was also identified. This result can help in designing new covalent inhibitors for SARS-CoV-2 M^{pro}, especially by focusing on increasing the exothermicity of that step.

COMPUTATIONAL METHODS

Preparation of the Simulation System. The catalytically active form of M^{pro} is a homodimer (Figure 2A). Therefore, a homodimer of the main protease (PDB entry 6Y2G)[7] was taken in all of our free energy calculations. Chain A of the homodimer was used as the main simulation system. The inhibitor in PDB entry 6Y2G (named **13b** in ref 7) (see Figure 2B) was used as the α-ketoamide inhibitor in our study. The covalent bond between the inhibitor and the sulfhydryl group of Cys145 was removed before starting any simulation. All of the nonprotein atoms except the inhibitor were removed from the PDB file. The protein was solvated using MOLARIS-XG[28] to generate a water sphere based on the surface constraint all-atom solvent model (SCAAS).[29] The simulation system was then energy minimized to remove any bad contacts in the protein system while keeping the coordinates of the inhibitor frozen. The partial charges of the inhibitor were calculated at the B3LYP/6-31+G** level of theory using Gaussian 09.[30] The charges obtained from the QM calculations were fitted using restrained electrostatic potential (RESP)[31] procedure to

https://dx.doi.org/10.1021/acs.biochem.0c00782
Biochemistry XXXX, XXX, XXX−XXX

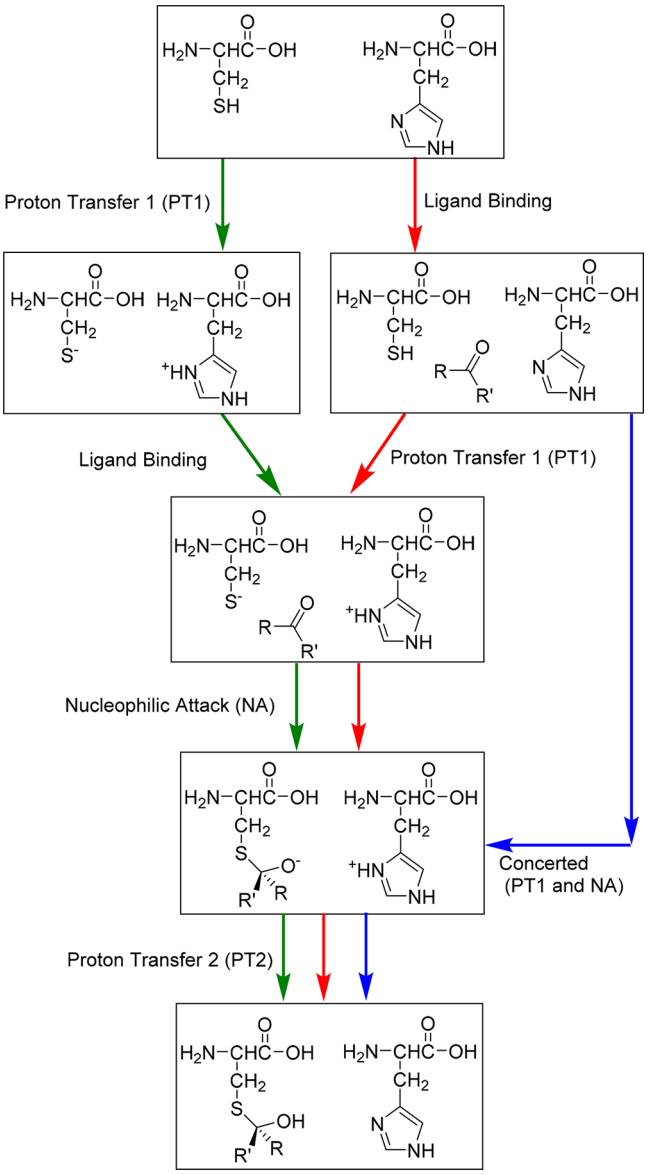

Figure 1. Various mechanistic schemes of formation of a covalent complex between a peptidomimetic inhibitor and a cysteine protease. The inhibitor is represented in generic form as RR′CO, where R and R′ can be any aliphatic or aromatic chain. The reacting molecular fragments are represented in boxes. The green, red, and blue arrows denote schemes A–C, respectively. The difference among schemes A–C is discussed in detail in the text.

obtain the RESP-based charges. In all of the simulations, the polarizable force field ENZYMIX[32] was used unless otherwise mentioned.

Empirical Valence Bond Simulations. In the EVB simulations, the reacting atoms are defined as region I atoms, while the rest of the protein atoms (up to a user-defined radius) are defined as region II. In some of our EVB simulations in which a few atoms of the inhibitor were included in region I, the geometric center of the inhibitor was considered as the center of the simulation system. On the contrary, in the simulations in which the atoms of the inhibitor were not part of region I, the geometric center of all of the protein atoms included in region I was used as the center. The protein–inhibitor system was immersed in a 22 Å sphere of water molecules. The water molecules at the boundary of the

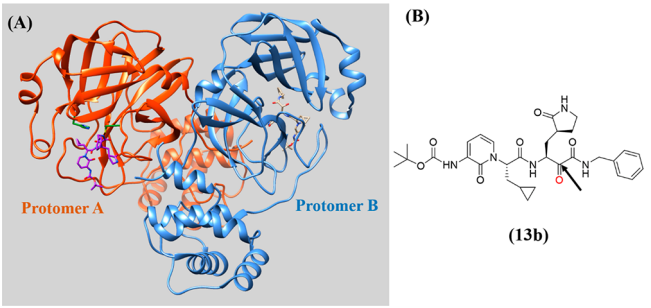

Figure 2. Structures of dimeric SARS-CoV-2 M^{pro} and its α-ketoamide inhibitor **13b**. (A) Protomers A and B are shown as orange and blue ribbons, respectively. The inhibitor and catalytic residues in protomer A are shown as purple and green sticks, respectively. (B) The most electrophilic center of **13b** is highlighted with a black arrow.

solvent sphere were subject to polarization and radial restraints by using the surface-constrained all-atom solvent (SCAAS) model. This simulation sphere was further surrounded by a 2 Å spherical shell of Langevin dipoles and then a bulk continuum. The long-range electrostatic effect was treated using the local reaction field (LRF) method.[33] All protein atoms beyond the 22 Å sphere were fixed at their initial coordinate positions as in the crystal structure. The electrostatic interaction from outside of the sphere was not included in the energy calculations. The partial charges of all region I atoms were calculated at the B3LYP/6-31+G** level of theory using Gaussian 09, and the partial charges and all other EVB parameters are provided in the Supporting Information.

Before the free energy surface (FES) was calculated using the EVB approach, the simulation system was equilibrated thoroughly. The temperature of the simulation system was increased slowly from 1 to 300 K in increments of 40 K (except from 280 to 300 K, where the increment was 20 K) for a total simulation time of 200 ps. During heating, the EVB region I atoms were constrained at 50 kcal/mol energy. This constraint was then released in six steps to 0.3 kcal/mol in an additional 100 ps. Finally, three different starting geometries were generated from an equilibration simulation of 300 ps. It is worth mentioning that the equilibration of a system is considerably fast with spherical boundary conditions. Additionally, we observed minimal fluctuation of the root-mean-square deviation (RMSD) of the positions of the heavy atoms in region II during the last 300 ps equilibrium simulations. In the EVB approach, the free energy surface is calculated using the free energy perturbation/umbrella sampling (FEP/US) method, and for that, we ran simulations of 51 frames with each frame simulated for 10 ps. For each reaction, the simulations of the reference reaction (a reaction in water without any protein atoms from region II) were also performed to obtain the necessary EVB parameters (gas phase shift and coupling constants). The definition of these parameters can be found in the Supporting Information. The reported energies in this work were obtained from the averaging of three independent EVB simulations.

PDLD/S-LRA/β Simulations. The simulation setup for the noncovalent binding energy was the same as that for the EVB simulations, except in the PDLD/S-LRA/β simulations, the whole inhibitor was included in region I and all atoms (including atoms in region I) in the simulation were represented with the ENZYMIX force field. Five different simulations (starting with different initial structures) were

https://dx.doi.org/10.1021/acs.biochem.0c00782
Biochemistry XXXX, XXX, XXX–XXX

performed for each noncovalent binding free energy calculation. The presented results were averages of those simulation results. In every PDLD/S-LRA/β simulation, the linear response approximation (LRA) calculation was performed on 10 different protein configurations. A brief description of the PDLD/S-LRA/ β method can be found in the Supporting Information.

RESULTS AND DISCUSSION

A generic binding process for a covalent inhibitor can be described formally as a two-step process, where the first step is formation of a noncovalent protein−inhibitor complex and the second step is the chemical reaction that forms a covalent protein−inhibitor complex (see Figure 3). As we can see from

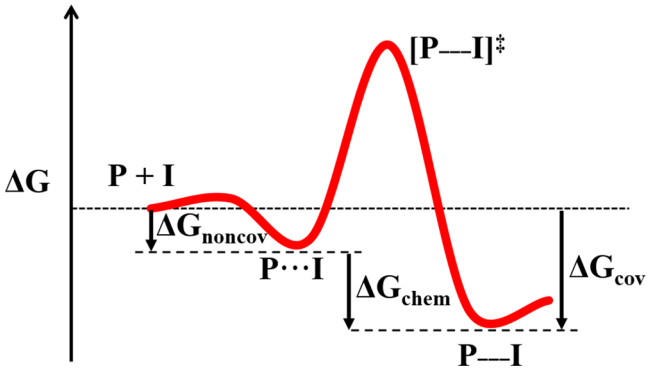

Figure 3. General free energy profile that explains the formation of a covalent protein (P)−inhibitor (I) complex. P···I, [P---I]‡, and P---I denote the noncovalent, activated complex(es) during chemical reaction(s) and the covalent binding state, respectively. ΔG_{noncov}, ΔG_{chem} , and ΔG_{cov} represent the noncovalent (P···I) binding energy, reaction free energy, and total covalent (P---I) binding free energy, respectively.

Figure 1, the chemical reaction can consist of multiple steps. Thus, the absolute binding free energy of a covalent complex can be a combination of many free energy terms. To compare the calculated covalent binding free energies with the corresponding experimental results, we need reliable calculations of each of those steps. In the following sections, we will discuss the calculations of the free energy changes for different steps, and finally, we will compare our calculated results with experimental results of inhibitor **13b**.

Noncovalent Binding Free Energy (ΔG_{noncov}) Calculations. M^{pro} with different ionization combinations was used to calculate the ΔG_{noncov} of two types of noncovalent complexes. In one case, we ionized all ionizable residues within 20 Å of the geometric center of the inhibitor as well as His41 (doubly protonated) and Cys145 (negatively charged), whereas in another case, the His41-Cys145 pair was kept in its neutral form. We have used the Monte Carlo Proton Transfer (MCPT)[34] method to assess the most probable ionization state of the titratable residues. The neutral form corresponds to the situation in which the inhibitor binding occurs before the proton transfer between Cys145 and His41. In this way, we have tested the hypothesis related to the ordering of the first proton transfer and inhibitor binding (schemes A and B in Figure 1). The calculated ΔG_{noncov} values are listed in Table 1. Interestingly, for inhibitor **13b** in both cases we obtained similar binding free energies. These results probably suggest that the ionization of Cys145 and His41 is not important for

Table 1. Calculated Binding Free Energies (ΔG_{noncov}) for the Noncovalent SARS-CoV-2 M^{pro}−13b Complexes

system	ΔG_{noncov} (kcal/mol)
13b (before proton transfer)	−3.5 ± 0.5
13b (after proton transfer)	−3.6 ± 0.5

the initial formation of the inhibitor−protein noncovalent complex. Crystal structures of the dimeric complexes of the mutated (C145A[35,36] or H41A[37]) M^{pro} of SARS-CoV-2 with bound C-terminal and N-terminal autocleavage substrates can be found in the literature. A bound substrate in those mutated (C145A or H41A) proteins indicates that the electrostatic influence of Cys145 and His41 might be nominal during the formation of the noncovalent complex. On the contrary, a more surprising part is such low values of ΔG_{noncov} for a large α-ketoamide inhibitor. Here we mention that the structures that were used to represent the noncovalent states were derived from coordinates of the covalent hemiketal form of the inhibitors. It is possible that in those structures the protein preorganization (which is mostly for stabilizing the transition state of covalent bond formation) is not sufficiently conducive to stabilize the noncovalent states. In other words, there is a possibility that the inhibitor binds in a mode slightly different than what has been simulated. At any rate, if we consider the chemical reaction step(s) along with this step, we could understand how strongly the exothermicity of the reactions drives the covalent complex formation despite the small ΔG_{noncov} contributions.

Calculating the Reaction Free Energy of the First Proton Transfer (PT1) Step. The investigation of the mechanism of covalent bond formation was started by evaluating the reaction free energy (ΔG_{PT1}) of the PT1 step. The PT1 reaction was simulated in the apo and holo forms of the protein. It should be noted that the calculations for the respective PT1 reactions in water (reference reactions) were also performed in the presence or absence of the inhibitor. The $\Delta G_{PT1,obs}$ of 7.0 kcal/mol in water (in the presence of the inhibitor) was taken from ref 38 to compare it with our calculated ΔG_{PT1} in water. In this case, it was assumed that the effect of the slightly different warheads of the inhibitors (reported in ref 38 and in this work) on the PT reaction is very similar. The $\Delta G_{PT1,obs}$ in water (in the absence of the inhibitor) was calculated from the pK_a values of ethanethiol (pK_a = 10.6) and imidazole (pK_a = 6.9). Here, the pK_a of ethanethiol instead of cysteine was taken, because in the case of cysteine, there is a main chain zwitterionic effect. Thus, the value of $\Delta G_{PT1,obs}$ in water (in absence of the ligand) is 1.38 × (10.6 − 6.9) = 5.1 kcal/mol. We used this value to compare our calculated EVB profile (in absence of the ligand) as well as to fit EVB parameters. The PT1 profiles obtained for the reactions in protein were different in the apo and holo forms of the protein (see Table 2). Table 2 shows that the His-Cys ion pair state is less favorable in the holo form of the protein than in the apo form, probably because the ion pair that forms at the end of the PT1 step is more stabilized in more polar environment like in the apo form (with a vacant inhibitor binding pocket) than in the holo form. Our results also match with those of ref 24, in which the proteolysis mechanism of SARS-CoV-2 was studied using multiscale DFT/MM simulation methods (see Table 2).

Calculation of the Activation and Reaction Free Energies of the Nucleophilic Attack (NA) Step. In the nucleophilic attack step, the activated anionic Sγ atom of

https://dx.doi.org/10.1021/acs.biochem.0c00782
Biochemistry XXXX, XXX, XXX−XXX

Table 2. Calculated Reaction Free Energies (ΔG_{PT1}) of the First Proton Transfer (PT1) Step in Water and SARS-CoV-2 M^{pro}

	system	ΔG_{PT1} (kcal/mol)	ΔG_{PT1} (kcal/mol)[a]
scheme A	water	5.1	–
	protein (apo)	2.9 ± 0.2	2.9
scheme B	water	7.5	–
	protein (holo)	7.3 ± 1.7	4.8

[a]The calculated reaction free energy from ref 24. Please note that in ref 24 a peptide substrate was used.

Cys145 attacks the α-keto group of the ketoamides and forms an anionic tetrahedral complex. In this case, the information about the observed activation ($\Delta G^{\ddagger}_{NA,obs}$) and reaction free energy ($\Delta G_{NA,obs}$) of the reference water reaction was taken from the free energy profiles reported in ref 38. It is worth mentioning that in ref 38 an amide system was used to study the free energy profile, whereas we have a ketoamide group. Thus, we also performed a QM-based energy calculation to estimate $\Delta G_{NA,obs}$ in water. From the QM calculations, we obtained a $\Delta G_{NA,obs}$ value of 12.8 kcal/mol (after adding the thermal corrections). The QM-calculated $\Delta G_{NA,obs}$ is close to the value reported in ref 38, and thus, we have used the exact PES as in ref 38 to parametrize our EVB simulations for the NA step. The calculated $\Delta G^{\ddagger}_{NA}$ and ΔG_{NA} are reported in Table 3.

Table 3. Calculated Activation ($\Delta G^{\ddagger}_{NA}$) and Reaction (ΔG_{NA}) Free Energies of the Nucleophilic Attack (NA) Step in Water and SARS-CoV-2 M^{pro}

	system	$\Delta G^{\ddagger}_{NA}$ (kcal/mol)	ΔG_{NA} (kcal/mol)
scheme A	water	17.7	12.6
	protein	13.5 ± 2.3	2.9 ± 2.2
scheme B	water	17.6	12.4
	protein	12.5 ± 0.9	−0.5 ± 1.7

In Table 3, two different values of ΔG_{NA} and $\Delta G^{\ddagger}_{NA}$ are reported, as we have explored two different stepwise mechanistic schemes (A and B). In scheme A, the PT1 step happens before the inhibitor binding, and we did not include His145 when we studied the NA step in the water environment (because this would help us to account for the effect of the protonated histidine residue in the protein reaction only). On the contrary, for scheme B, we performed a continuation of a run from the previous PT1 run. Thus, the His145 residue was included in water and protein reactions for the NA step. Thus, the effect of His145 was incorporated slightly differently in the simulations of these schemes (A and B). Although the representations of the simulation systems are slightly different, the total free energy change of the three steps (ΔG_{noncov} + ΔG_{PT1} + ΔG_{NA}) should converge for both schemes. The calculated free energy changes after the first three steps are 3.3 and 2.2 kcal/mol for schemes A and B, respectively. Thus, the process after the first three steps is endothermic even in the protein. This indicates that the major exothermicity observed due to the formation of the covalent inhibitor−protein complex should come from the last proton transfer step.

At this point, we discuss the third mechanistic scheme considered in this study. In ref 23, the author proposed that the first proton transfer occurs concomitantly with the nucleophilic attack step. For our PT1 free energy surface calculations, it was also observed that in the presence of the inhibitor the Cys-His ion pair (product of PT1) was more unstable compared to that when the inhibitor was absent. Thus, it is quite possible that the nucleophilic attack happens almost immediately after the formation of the less stable ion pair in the holo form of the protein. Therefore, a concerted PT1 and NA step is a legitimate option to check.

Calculation of Activation and Reaction Free Energies of the Concerted PT1 and NA Step. The results for the concerted step are presented in Table 4. To parametrize the

Table 4. Calculated Activation ($\Delta G^{\ddagger}_{PT1-NA}$) and Reaction ($\Delta G_{PT1-NA}$) Free Energies of the Concerted PT1 and NA Step in Water and SARS-CoV-2 M^{pro}

	system	$\Delta G^{\ddagger}_{PT1-NA}$ (kcal/mol)	ΔG_{PT1-NA} (kcal/mol)
scheme C	water	24.4	18.6
	protein	13.6 ± 0.2	6.1 ± 0.8

EVB simulation, here we also performed EVB simulations of the reference reaction in water. For the reference reaction, it was assumed that the observed activation barrier ($\Delta G^{\ddagger}_{PT1-NA,obs}$) and reaction free energy ($\Delta G_{PT1-NA,obs}$) of the concerted reaction are the same as those of the stepwise reaction discussed in ref 38, and values of 24 and 19 kcal/mol, respectively, were used for the free energy changes. The calculated barrier of the concerted reaction (in scheme C) is 13.6 kcal/mol (Table 4), whereas for the stepwise process, the combined barriers (including PT1 and NA) are 16.4 and 19.8 kcal/mol for schemes A and B, respectively (Tables 2 and 3). Thus, we can conclude that scheme C provides a more plausible mechanism. On the contrary, the total changes in reaction free energies (ΔG_{noncov} + ΔG_{PT1-NA} or ΔG_{noncov} + ΔG_{PT1} + ΔG_{NA}) for the formation of the anionic tetrahedral complex are comparable in all three schemes. This confirms the consistency in our simulations.

Calculation of the Reaction Free Energy of the Second Proton Transfer (PT2) Step. The last proton transfer step is common for all three mechanistic schemes. To obtain the observed reaction free energy ($\Delta G_{PT2,obs}$) for the reaction in water, here we have also used the information about the pK_a's of the reacting groups. The obtained $\Delta G_{PT2,obs}$ in water was −5.6 kcal/mol considering the pK_a of imidazole (6.9) and the pK_a of the tetrahedral intermediate[38] (∼11.0). The calculated results for the reaction in the protein and water are listed in Table 5.

Table 5. Calculated Reaction Free Energies (ΔG_{PT2}) of the Second Proton Transfer Step (PT2) in Water and SARS-CoV-2 M^{pro}

system	ΔG_{PT2} (kcal/mol)
water	−5.6
protein	−11.4 ± 0.9

The results in Table 5 suggest that the proton affinity of the tetrahedral complex is very important (along with the electrophilicity of the reacting group of the inhibitor) in designing an inhibitor that is better than that of **13b**, because the PT2 step contributes to the maximum exothermicity during covalent bond formation. Recently, two mechanistic studies[39,40] of the inhibition of M^{pro} have been reported, where a peptidyl Michael acceptor N3 was used as the covalent

https://dx.doi.org/10.1021/acs.biochem.0c00782
Biochemistry XXXX, XXX, XXX−XXX

inhibitor. In both works, the last proton transfer step has been reported to be highly exothermic, which is in agreement with our study. Additionally, the reported activation free energy of the covalent bond formation step in ref 39 is close to what we have obtained here. In another study, Arafet et al.[41] reported that the protonated hemiketal intermediate of halomethyl ketone inhibitors of cruzain (a cysteine protease) was highly stable compared to that of the anion forms. Although in their study the second proton transfer preceded or happened concurrently with the nucleophilic attack, it produced the same conclusion about the contribution of the second proton transfer step to the overall exothermicity, as we have found here.

Calculation of the Binding Free Energy of the Covalent SARS-CoV-2 Inhibitor Complex. Finally, we can add all of the calculated free energy contributions to obtain the binding free energy (ΔG_{cov}) of the covalent complex between M^{pro} and inhibitor **13b**. The experimental IC_{50} value for **13b** is 0.67 μM.[7] Therefore, the experimental binding free energy at 300 K can be estimated as −8.5 kcal/mol. The total free energy change for each reaction scheme is reported in Table 6, and the overall free energy profiles for the formation of the covalent complex between SARS-CoV-2 M^{pro} and inhibitor **13b** (following different mechanistic schemes) are depicted in Figure 4. It can be seen from Table 6 that the calculated ΔG_{cov} is close to the experimental ΔG_{cov}.

Table 6. Calculated (ΔG_{cov}^{cal}) and Experimental (ΔG_{cov}^{exp}) Binding Free Energies of the Covalent SARS-CoV-2 M^{pro}−Inhibitor 13b Complex

scheme	ΔG_{cov}^{cal} (kcal/mol)	ΔG_{cov}^{exp} (kcal/mol)[a]
A	−9.2	−8.5
B	−8.1	
C	−8.9	

[a] ΔG_{cov}^{exp} is calculated from the IC_{50} value reported in ref 7.

However, it is worth mentioning that the IC_{50} value is not the best metric for evaluating the accuracy of a protocol for absolute binding free energy calculations. Despite that, due to the lack of an experimentally reported K_i (inhibition constant) value for the α-ketoamide inhibitor **13b**, we had to use the IC_{50} value, an indirect metric of binding affinity, for our study. It is known that the relationship between K_i and IC_{50} depends on the experimental condition and on the binding affinity of the substrate (K_M). In general, the K_i value is equal or less than the IC_{50} value;[42] thus, the actual binding affinity of **13b** should be even lower than −8.5 kcal/mol. On the contrary, **13b** is known to be a reversible covalent inhibitor. For similar reversible α-ketoamide inhibitors of calpains and other cysteine proteases, the reported K_i values[43] were around 15 nM and the corresponding binding free energy will be −11 kcal/mol. Therefore, the expected value may be 3−4 kcal/mol more negative than what we can obtain from the IC_{50} value of **13b**. At any rate, we think our estimated absolute binding free energy of the M^{pro}−**13b** covalent complex is not significantly over- or underestimated and we can also account for the fact that **13b** is not an irreversible inhibitor.

The reversibility of a reaction depends generally on the barrier of the reverse reaction. For two reactions with comparable activation barriers, the reaction that is more exothermic is also more irreversible. Thus, the calculated reaction free energies of two reactions can be used to determine whether a covalent inhibitor is reversible.[44] On the contrary, reactions with high reverse reaction barriers are irreversible even if the exothermicity is small. It is known that reversible covalent inhibitors can have a residence time (τ = 10 h)[45] which is equivalent to a reverse reaction barrier of around 23.5 kcal/mol. We have obtained a reverse reaction barrier of around 22 kcal/mol combining the NA and PT2 steps, which supports the idea that the protonated tetrahedral complex of **13b** can undergo a reverse reaction to form the noncovalent complex. At this point, we caution that the time dependence of the binding process has not been provided in the experimental work and thus it is not completely clear that our assumption about the thermodynamic equilibrium is fully justified.

CONCLUSIONS

The great potential of covalently bound drugs has been demonstrated in recent years.[46−49] Still, most current approaches to *in silico* design of such inhibitors are not fully consistent for absolute binding free energy calculations, because they do not evaluate the chemical contribution of the binding energy. We developed a general way to calculate the binding free energies of covalent drugs, including all of the relevant energy contributions. That is, our strategy is based on using the EVB to evaluate the chemical contribution for covalent binding and using the PDLD/S-LRA/β method to

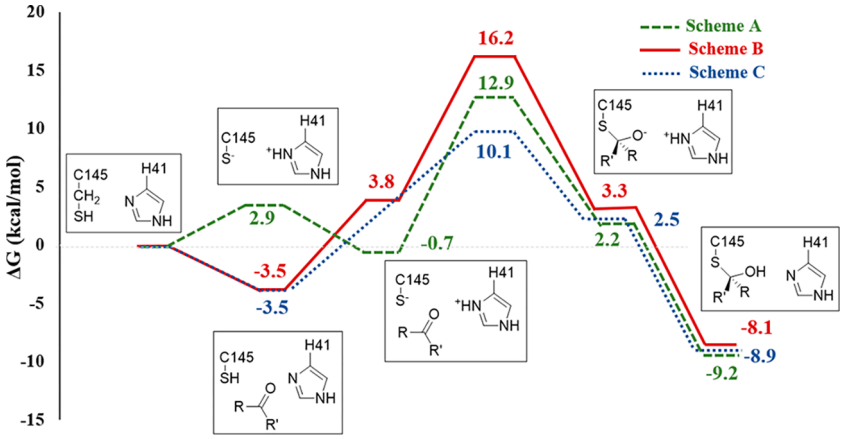

Figure 4. Free energy surface (FES) of formation of the covalent protein ligand (SARS-CoV-2 M^{pro}−**13b**) complex. The boxes near the surfaces represent the reaction coordinate at the corresponding position of the FES.

https://dx.doi.org/10.1021/acs.biochem.0c00782
Biochemistry XXXX, XXX, XXX−XXX

determine the noncovalent contribution. This approach is examined by calculating the binding free energy of an α-ketoamide inhibitor of the main protease of SARS-CoV-2 ($M^{pro.}$). Our calculations considered multiple reaction pathways for inhibitor−protease complex formation and produced a very reasonable estimate of the observed binding free energy. This demonstrated the potential of our strategy in general drug design and particularly in looking for effective inhibitors for SARS-CoV-2.

■ ASSOCIATED CONTENT

Supporting Information

The Supporting Information is available free of charge at https://pubs.acs.org/doi/10.1021/acs.biochem.0c00782.

All relevant EVB simulation parameters and partial charges (Tables S2.1−S2.4) (PDF)

■ AUTHOR INFORMATION

Corresponding Author

Arieh Warshel − *Department of Chemistry, University of Southern California, Los Angeles, California 90089, United States;* orcid.org/0000-0001-7971-5401; Email: warshel@usc.edu

Author

Dibyendu Mondal − *Department of Chemistry, University of Southern California, Los Angeles, California 90089, United States;* orcid.org/0000-0002-5047-6985

Complete contact information is available at: https://pubs.acs.org/10.1021/acs.biochem.0c00782

Funding

This work was supported by National Institutes of Health Grant R35 GM122472 and National Science Foundation Grant MCB 1707167.

Notes

The authors declare no competing financial interest.

■ ACKNOWLEDGMENTS

The authors thank the University of Southern California for the Zumberge Multi-School Interdisciplinary Research award and the University of Southern California High Performance Computing and Communication Center and the Extreme Science and Engineering Discovery Environment's (XSEDE) Comet facility at the San Diego Supercomputing Center for computational resources. D.M. thanks Dr. Gabriel Oanca for helpful discussion.

■ REFERENCES

(1) Zhou, P., Yang, X. L., Wang, X. G., Hu, B., Zhang, L., Zhang, W., Si, H. R., Zhu, Y., Li, B., Huang, C. L., Chen, H. D., Chen, J., Luo, Y., Guo, H., Jiang, R. D., Liu, M. Q., Chen, Y., Shen, X. R., Wang, X., Zheng, X. S., Zhao, K., Chen, Q. J., Deng, F., Liu, L. L., Yan, B., Zhan, F. X., Wang, Y. Y., Xiao, G. F., and Shi, Z. L. (2020) A pneumonia outbreak associated with a new coronavirus of probable bat origin. *Nature 579* (7798), 270−273.

(2) Wu, F., Zhao, S., Yu, B., Chen, Y. M., Wang, W., Song, Z. G., Hu, Y., Tao, Z. W., Tian, J. H., Pei, Y. Y., Yuan, M. L., Zhang, Y. L., Dai, F. H., Liu, Y., Wang, Q. M., Zheng, J. J., Xu, L., Holmes, E. C., and Zhang, Y. Z. (2020) A new coronavirus associated with human respiratory disease in China. *Nature 579* (7798), 265−269.

(3) Gorbalenya, A. E., Baker, S. C., Baric, R. S., de Groot, R. J., Drosten, C., Gulyaeva, A. A., Haagmans, B. L., Lauber, C., Leontovich, A. M., Neuman, B. W., Penzar, D., Perlman, S., Poon, L. L. M., Samborskiy, D. V., Sidorov, I. A., Sola, I., Ziebuhr, J., and Grp, C. S. (2020) The species Severe acute respiratory syndrome-related coronavirus: classifying 2019-nCoV and naming it SARS-CoV-2. *Nat. Microbiol. 5* (4), 536−544.

(4) Guy, R. K., DiPaola, R. S., Romanelli, F., and Dutch, R. E. (2020) Rapid repurposing of drugs for COVID-19. *Science 368* (6493), 829−830.

(5) Anand, K., Ziebuhr, J., Wadhwani, P., Mesters, J. R., and Hilgenfeld, R. (2003) Coronavirus main proteinase (3CL(pro)) structure: Basis for design of anti-SARS drugs. *Science 300* (5626), 1763−1767.

(6) Chang, G. G. (2010) Quaternary Structure of the SARS Coronavirus Main Protease. *Molecular Biology of the Sars-Coronavirus*, 115−128.

(7) Zhang, L. L., Lin, D. Z., Sun, X. Y. Y., Curth, U., Drosten, C., Sauerhering, L., Becker, S., Rox, K., and Hilgenfeld, R. (2020) Crystal structure of SARS-CoV-2 main protease provides a basis for design of improved alpha-ketoamide inhibitors. *Science 368* (6489), 409−412.

(8) Jin, Z. M., Du, X. Y., Xu, Y. C., Deng, Y. Q., Liu, M. Q., Zhao, Y., Zhang, B., Li, X. F., Zhang, L. K., Peng, C., Duan, Y. K., Yu, J., Wang, L., Yang, K. L., Liu, F. J., Jiang, R. D., Yang, X. L., You, T., Liu, X. C., Yang, X. N., Bai, F., Liu, H., Liu, X., Guddat, L. W., Xu, W. Q., Xiao, G. F., Qin, C. F., Shi, Z. L., Jiang, H. L., Rao, Z. H., and Yang, H. T. (2020) Structure of M-pro from SARS-CoV-2 and discovery of its inhibitors. *Nature 582* (7811), 289−293.

(9) Jin, Z. M., Zhao, Y., Sun, Y., Zhang, B., Wang, H. F., Wu, Y., Zhu, Y., Zhu, C., Hu, T. Y., Du, X. Y., Duan, Y. K., Yu, J., Yang, X. B., Yang, X. N., Yang, K. L., Liu, X., Guddat, L. W., Xiao, G. F., Zhang, L. K., Yang, H. T., and Rao, Z. H. (2020) Structural basis for the inhibition of SARS-CoV-2 main protease by antineoplastic drug carmofur. *Nat. Struct. Mol. Biol. 27* (6), 529−532.

(10) Dai, W. H., Zhang, B., Jiang, X. M., Su, H. X., Li, J. A., Zhao, Y., Xie, X., Jin, Z. M., Peng, J. J., Liu, F. J., Li, C. P., Li, Y., Bai, F., Wang, H. F., Cheng, X., Cen, X. B., Hu, S. L., Yang, X. N., Wang, J., Liu, X., Xiao, G. F., Jiang, H. L., Rao, Z. H., Zhang, L. K., Xu, Y. C., Yang, H. T., and Liu, H. (2020) Structure-based design of antiviral drug candidates targeting the SARS-CoV-2 main protease. *Science 368* (6497), 1331−1335.

(11) Powers, J. C., Asgian, J. L., Ekici, O. D., and James, K. E. (2002) Irreversible inhibitors of serine, cysteine, and threonine proteases. *Chem. Rev. 102* (12), 4639−4750.

(12) Zhang, L. L., Lin, D. Z., Kusov, Y., Nian, Y., Ma, Q. J., Wang, J., von Brunn, A., Leyssen, P., Lanko, K., Neyts, J., de Wilde, A., Snijder, E. J., Liu, H., and Hilgenfeld, R. (2020) alpha-Ketoamides as Broad-Spectrum Inhibitors of Coronavirus and Enterovirus Replication: Structure-Based Design, Synthesis, and Activity Assessment. *J. Med. Chem. 63* (9), 4562−4578.

(13) Mondal, D., Florian, J., and Warshel, A. (2019) Exploring the Effectiveness of Binding Free Energy Calculations. *J. Phys. Chem. B 123* (42), 8910−8915.

(14) Wang, L., Wu, Y. J., Deng, Y. Q., Kim, B., Pierce, L., Krilov, G., Lupyan, D., Robinson, S., Dahlgren, M. K., Greenwood, J., Romero, D. L., Masse, C., Knight, J. L., Steinbrecher, T., Beuming, T., Damm, W., Harder, E., Sherman, W., Brewer, M., Wester, R., Murcko, M., Frye, L., Farid, R., Lin, T., Mobley, D. L., Jorgensen, W. L., Berne, B. J., Friesner, R. A., and Abel, R. (2015) Accurate and Reliable Prediction of Relative Ligand Binding Potency in Prospective Drug Discovery by Way of a Modern Free-Energy Calculation Protocol and Force Field. *J. Am. Chem. Soc. 137* (7), 2695−2703.

(15) Chatterjee, P., Botello-Smith, W. M., Zhang, H., Qian, L., Alsamarah, A., Kent, D., Lacroix, J. J., Baudry, M., and Luo, Y. (2017) Can Relative Binding Free Energy Predict Selectivity of Reversible Covalent Inhibitors? *J. Am. Chem. Soc. 139* (49), 17945−17952.

(16) Yu, H. S., Gao, C., Lupyan, D., Wu, Y. J., Kimura, T., Wu, C. J., Jacobson, L., Harder, E., Abel, R., and Wang, L. L. (2019) Toward Atomistic Modeling of Irreversible Covalent Inhibitor Binding Kinetics. *J. Chem. Inf. Model. 59* (9), 3955−3967.

(17) Kuhn, B., Tichy, M., Wang, L. L., Robinson, S., Martin, R. E., Kuglstatter, A., Benz, J., Giroud, M., Schirmeister, T., Abel, R., Diederich, F., and Hert, J. (2017) Prospective Evaluation of Free Energy Calculations for the Prioritization of Cathepsin L Inhibitors. *J. Med. Chem. 60* (6), 2485−2497.
(18) Lameira, J., Bonatto, V., Cianni, L., dos Reis Rocho, F., Leitao, A., and Montanari, C. A. (2019) Predicting the affinity of halogenated reversible covalent inhibitors through relative binding free energy. *Phys. Chem. Chem. Phys. 21* (44), 24723−24730.
(19) Zhang, H., Jiang, W. J., Chatterjee, P., and Luo, Y. (2019) Ranking Reversible Covalent Drugs: From Free Energy Perturbation to Fragment Docking. *J. Chem. Inf. Model. 59* (5), 2093−2102.
(20) Singh, N., and Warshel, A. (2010) Absolute binding free energy calculations: On the accuracy of computational scoring of protein-ligand interactions. *Proteins: Struct., Funct., Genet. 78* (7), 1705−1723.
(21) Warshel, A., and Weiss, R. M. (1980) An Empirical Valence Bond Approach for Comparing Reactions in Solutions and in Enzymes. *J. Am. Chem. Soc. 102* (20), 6218−6226.
(22) Jindal, G., Mondal, D., and Warshel, A. (2017) Exploring the Drug Resistance of HCV Protease. *J. Phys. Chem. B 121* (28), 6831−6840.
(23) Świderek, K., and Moliner, V. (2020) Revealing the molecular mechanisms of proteolysis of SARS-CoV-2 M pro by QM/MM computational methods. *Chem. Sci. 11*, 10626−10630.
(24) Ramos-Guzmán, C. A., Ruiz-Pernía, J. J., and Tuñón, I. (2020) Unraveling the SARS-CoV-2 Main Protease Mechanism Using Multiscale DFT/MM Methods. *chemRxiv*, DOI: 10.26434/chemrxiv.12501734.v2.
(25) Polgár, L. (1973) On the mode of activation of the catalytically essential sulfhydryl group of papain. *Eur. J. Biochem. 33* (1), 104−109.
(26) Huang, C. K., Wei, P., Fan, K. Q., Liu, Y., and Lai, L. H. (2004) 3C-like proteinase from SARS coronavirus catalyzes substrate hydrolysis by a general base mechanism. *Biochemistry 43* (15), 4568−4574.
(27) Connolly, K. M., Smith, B. T., Pilpa, R., Ilangovan, U., Jung, M. E., and Clubb, R. T. (2003) Sortase from Staphylococcus aureus does not contain a thiolate-imidazolium ion pair in its active site. *J. Biol. Chem. 278* (36), 34061−34065.
(28) Warshel, A., Chu, Z., Villa, J., Strajbl, M., Schutz, C., Shurki, A., Vicatos, S., Plotnikov, N., and Schopf, P. (2012) *Molaris-XG*, ver. 9.15, University of Southern California, Los Angeles.
(29) King, G., and Warshel, A. (1989) A Surface Constrained All-Atom Solvent Model for Effective Simulations of Polar Solutions. *J. Chem. Phys. 91* (6), 3647−3661.
(30) Frisch, M. J., Trucks, G. W., Schlegel, H. B., Scuseria, G. E., Robb, M. A., Cheeseman, J. R., Scalmani, G., Barone, V., Mennucci, B., Petersson, G., et al. (2014) *Gaussian 09*, rev. D.01, Gaussian, Inc., Wallingford, CT.
(31) Bayly, C. I., Cieplak, P., Cornell, W. D., and Kollman, P. A. (1993) A Well-Behaved Electrostatic Potential Based Method Using Charge Restraints for Deriving Atomic Charges - the Resp Model. *J. Phys. Chem. 97* (40), 10269−10280.
(32) Lee, F. S., Chu, Z. T., and Warshel, A. (1993) Microscopic and Semimicroscopic Calculations of Electrostatic Energies in Proteins by the Polaris and Enzymix Programs. *J. Comput. Chem. 14* (2), 161−185.
(33) Lee, F. S., and Warshel, A. (1992) A Local Reaction Field Method for Fast Evaluation of Long-Range Electrostatic Interactions in Molecular Simulations. *J. Chem. Phys. 97* (5), 3100−3107.
(34) Vorobyov, I., Kim, I., Chu, Z. T., and Warshel, A. (2016) Refining the treatment of membrane proteins by coarse-grained models. *Proteins: Struct., Funct., Genet. 84* (1), 92−117.
(35) Hsu, M. F., Kuo, C. J., Chang, K. T., Chang, H. C., Chou, C. C., Ko, T. P., Shr, H. L., Chang, G. G., Wang, A. H. J., and Liang, P. H. (2005) Mechanism of the maturation process of SARS-CoV 3CL protease. *J. Biol. Chem. 280* (35), 31257−31266.
(36) Muramatsu, T., Takemoto, C., Kim, Y. T., Wang, H. F., Nishii, W., Terada, T., Shirouzu, M., and Yokoyama, S. (2016) SARS-CoV 3CL protease cleaves its C-terminal autoprocessing site by novel subsite cooperativity. *Proc. Natl. Acad. Sci. U. S. A. 113* (46), 12997−13002.
(37) Xue, X. Y., Yu, H. W., Yang, H. T., Xue, F., Wu, Z. X., Shen, W., Li, J., Zhou, Z., Ding, Y., Zhao, Q., Zhang, X. J. C., Liao, M., Bartlam, M., and Rao, Z. (2008) Structures of two coronavirus main proteases: Implications for substrate binding and antiviral drug design. *J. Virol. 82* (5), 2515−2527.
(38) Strajbl, M., Florian, J., and Warshel, A. (2001) Ab initio evaluation of the free energy surfaces for the general base/acid catalyzed thiolysis of formamide and the hydrolysis of methyl thiolformate: A reference solution reaction for studies of cysteine proteases. *J. Phys. Chem. B 105* (19), 4471−4484.
(39) Arafet, K., Serrano-Aparicio, N., Lodola, A., Mulholland, A., González, F. V., Swiderek, K., and Moliner, V. (2020) Mechanism of Inhibition of SARS-CoV-2 Mpro by N3 Peptidyl Michael Acceptor Explained by QM/MM Simulations and Design of New Derivatives with Tunable Chemical Reactivity. *chemRxiv*, DOI: 10.26434/chemrxiv.12941819.v1.
(40) Ramos-Guzmán, C. A., Ruiz-Pernía, J. J., and Tuñón, I. (2020) A Microscopic Description of SARS-CoV-2 Main Protease Inhibition with Michael Acceptors. Strategies for Improving Inhibitors Design. *chemRxiv*, DOI: 10.26434/chemrxiv.12895064.v1.
(41) Arafet, K., Ferrer, S., and Moliner, V. (2015) First quantum mechanics/molecular mechanics studies of the inhibition mechanism of cruzain by peptidyl halomethyl ketones. *Biochemistry 54* (21), 3381−3391.
(42) Brandt, R. B., Laux, J. E., and Yates, S. W. (1987) Calculation of Inhibitor Ki and Inhibitor Type from the Concentration of Inhibitor for 50-Percent Inhibition for Michaelis-Menten Enzymes. *Biochem. Med. Metab. Biol. 37* (3), 344−349.
(43) Li, Z. Z., OrtegaVilain, A. C., Patil, G. S., Chu, D. L., Foreman, J. E., Eveleth, D. D., and Powers, J. C. (1996) Novel peptidyl alpha-keto amide inhibitors of calpains and other cysteine proteases. *J. Med. Chem. 39* (20), 4089−4098.
(44) da Costa, C. H. S., Bonatto, V., dos Santos, A. M., Lameira, J., Leitao, A., and Montanari, C. A. (2020) Evaluating QM/MM Free Energy Surfaces for Ranking Cysteine Protease Covalent Inhibitors. *J. Chem. Inf. Model. 60* (2), 880−889.
(45) Abdeldayem, A., Raouf, Y. S., Constantinescu, S. N., Moriggl, R., and Gunning, P. T. (2020) Advances in covalent kinase inhibitors. *Chem. Soc. Rev. 49* (9), 2617−2687.
(46) Lanman, B. A., Allen, J. R., Allen, J. G., Amegadzie, A. K., Ashton, K. S., Booker, S. K., Chen, J. J., Chen, N., Frohn, M. J., Goodman, G., Kopecky, D. J., Liu, L., Lopez, P., Low, J. D., Ma, V., Minatti, A. E., Nguyen, T. T., Nishimura, N., Pickrell, A. J., Reed, A. B., Shin, Y., Siegmund, A. C., Tamayo, N. A., Tegley, C. M., Walton, M. C., Wang, H. L., Wurz, R. P., Xue, M., Yang, K. C., Achanta, P., Bartberger, M. D., Canon, J., Hollis, L. S., McCarter, J. D., Mohr, C., Rex, K., Saiki, A. Y., San Miguel, T., Volak, L. P., Wang, K. H., Whittington, D. A., Zech, S. G., Lipford, J. R., and Cee, V. J. (2020) Discovery of a Covalent Inhibitor of KRAS(G12C) (AMG 510) for the Treatment of Solid Tumors. *J. Med. Chem. 63* (1), 52−65.
(47) Ghosh, A. K., Samanta, I., Mondal, A., and Liu, W. R. (2019) Covalent Inhibition in Drug Discovery. *ChemMedChem 14* (9), 889−906.
(48) Byrd, J. C., Harrington, B., O'Brien, S., Jones, J. A., Schuh, A., Devereux, S., Chaves, J., Wierda, W. G., Awan, F. T., Brown, J. R., et al. (2016) Acalabrutinib (ACP-196) in relapsed chronic lymphocytic leukemia. *N. Engl. J. Med. 374* (4), 323−332.
(49) Bradshaw, J. M., McFarland, J. M., Paavilainen, V. O., Bisconte, A., Tam, D., Phan, V. T., Romanov, S., Finkle, D., Shu, J., Patel, V., Ton, T., Li, X. Y., Loughhead, D. G., Nunn, P. A., Karr, D. E., Gerritsen, M. E., Funk, J. O., Owens, T. D., Verner, E., Brameld, K. A., Hill, R. J., Goldstein, D. M., and Taunton, J. (2015) Prolonged and tunable residence time using reversible covalent kinase inhibitors. *Nat. Chem. Biol. 11* (7), 525−531.

https://dx.doi.org/10.1021/acs.biochem.0c00782
Biochemistry XXXX, XXX, XXX−XXX